NASA/TM–20230000169

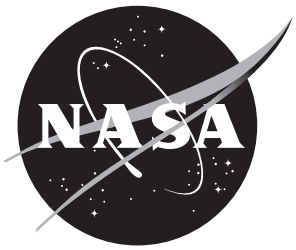

BOLT II Forebody Surface Measurement Analysis

Andrew N. Leidy
Langley Research Center, Hampton, Virginia

January 2023

NASA STI Program. . . in Profile

Since its founding, NASA has been dedicated to the advancement of aeronautics and space science. The NASA scientific and technical information (STI) program plays a key part in helping NASA maintain this important role.

The NASA STI Program operates under the auspices of the Agency Chief Information Officer. It collects, organizes, provides for archiving, and disseminates NASA's STI. The NASA STI Program provides access to the NASA Aeronautics and Space Database and its public interface, the NASA Technical Report Server, thus providing one of the largest collection of aeronautical and space science STI in the world. Results are published in both non-NASA channels and by NASA in the NASA STI Report Series, which includes the following report types:

- TECHNICAL PUBLICATION. Reports of completed research or a major significant phase of research that present the results of NASA programs and include extensive data or theoretical analysis. Includes compilations of significant scientific and technical data and information deemed to be of continuing reference value. NASA counterpart of peer-reviewed formal professional papers, but having less stringent limitations on manuscript length and extent of graphic presentations.
- TECHNICAL MEMORANDUM. Scientific and technical findings that are preliminary or of specialized interest, e.g., quick release reports, working papers, and bibliographies that contain minimal annotation. Does not contain extensive analysis.
- CONTRACTOR REPORT. Scientific and technical findings by NASA-sponsored contractors and grantees.
- CONFERENCE PUBLICATION. Collected papers from scientific and technical conferences, symposia, seminars, or other meetings sponsored or co-sponsored by NASA.
- SPECIAL PUBLICATION. Scientific, technical, or historical information from NASA programs, projects, and missions, often concerned with subjects having substantial public interest.
- TECHNICAL TRANSLATION. English-language translations of foreign scientific and technical material pertinent to NASA's mission.

Specialized services also include organizing and publishing research results, distributing specialized research announcements and feeds, providing information desk and personal search support, and enabling data exchange services.

For more information about the NASA STI Program, see the following:

- Access the NASA STI program home page at `http://www.sti.nasa.gov`
- E-mail your question to `help@sti.nasa.gov`
- Phone the NASA STI Information Desk at 757-864-9658
- Write to:
  NASA STI Information Desk
  Mail Stop 148
  NASA Langley Research Center
  Hampton, VA 23681-2199

NASA/TM–20230000169

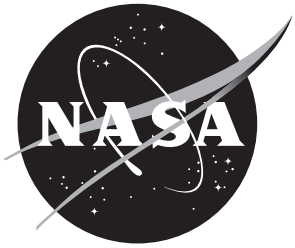

BOLT II Forebody Surface Measurement Analysis

Andrew N. Leidy
Langley Research Center, Hampton, Virginia

National Aeronautics and
Space Administration

Langley Research Center
Hampton, Virginia 23681-2199

January 2023

Available from:

NASA STI Program / Mail Stop 148
NASA Langley Research Center
Hampton, VA 23681-2199
Fax: 757-864-6500

Abstract

Surface impression molds of the nosetip/forebody interface, discrete tripping elements, and other surface imperfections were formed on the BOLT II flight vehicle prior to its launch in March 2022. The silicon-rubber molds cast on the interface between the nickel nosetip and the stainless steel forebody were measured using a 3D optical measurement system and a stylus profilometer and were evaluated for step direction and height. The step around the nosetip/forebody interface was found to vary in both magnitude and direction, but values were generally modest with most samples below 60 μm across the span and only two samples, both cast in the gutter, with step values larger than 100 μm. Impressions of the secondary-side tripping elements were strictly scanned with the optical device and similar methods were used to calculate trip height as step height. The measured centerline trip height was 2623 $\pm$12 μm, while the leading-edge, quadrant 2 and 3, trip heights were 897 $\pm$5 μm and 891 $\pm$18 μm, respectively. Surface imperfections on the nose and forebody were also evaluated. Surface roughness values and spectra were estimated, and profiles were extracted across the imperfections to quantify the magnitude of those features.

Contents

1 Introduction

The BOLT II in Memory of Mike Holden flight experiment was designed to advance the understanding and modeling of hypersonic turbulent boundary layers on concave surfaces with swept leading edges [1, 2]. The primary surface of the model featured naturally occurring transition, while the secondary surface was tripped using discrete roughness elements. Surface impressions were made on key features of the flight vehicle at room temperature several weeks prior to flight. The molds were previously described by McKiernan and Butler through private correspondence in the unpublished document "BOLT II Forebody Surface Measurements," and much of that information is included herein. A convention was established in that document to define where the molds were cast. The model was divided into quadrants as sketched in Fig. 1. Quadrants 1 and 4 are located on the primary side of the model, while quadrants 2 and 3 are on the secondary, tripped side. A picture of the full model with the secondary side facing up is shown in Fig. 2. A total of 20 impressions were made along the perimeter of the interface between the nickel 201 nosetip and the 410 stainless steel forebody, located 18.5 cm downstream of the nose leading edge. The letters A–F define the relative position of the sample within each quadrant, with A centered on the experimental surface, D on the leading edge, and F centered on the gutter. The relative positions are further defined in Table 1. The name of each mold is a combination of quadrant and relative position. Samples taken on the border of two quadrants are named with both quadrants listed. For example, sample Q1-4 A was taken on the experimental centerline on the primary side of the model.

Section 2 describes the methods of measurement using both the optical system and the stylus profilometer. Section 3 details the methods of analysis, particularly the process for calculating the step height. Section 4 reports the results, and Section 5 presents a summary and some conclusions.

2 Methods of Measurement

2.1 3D Optical

Each surface impression mold was measured using a structured-light-based, wide-area 3D system, which provided a 24.0 x 18.0 mm mapping of surface height with 23.5 μm/px spatial resolution. The stated accuracy of the measurement height values is ± 3 μm. Each of the 20 inferface-step samples was oriented so that the seam from the step was vertical or horizontal in the viewing area with most of the sample contained in the image. The measurement system has the ability to stitch images together; however, that capability was not utilized for evaluating the step height. Some samples had to be rotated 90 degrees or slightly tilted to maximize the area that the unit was able to measure. Data were not obtainable for regions where the sample angle was too oblique relative to the detector or if the angle was normal but the region was too reflective. A rectangular area just upstream of the step was defined as zero reference height for each sample. The tripping element samples were imaged with the trip centered in the field of view, and an area of the field outside of

the trip was set as the reference zero. The samples were positioned to best capture the pertinent features on the remaining surface imperfection molds.

The system also uses RGB light from a dedicated unit to produce detailed color images. Those photographs for all 20 interface step molds are presented in Figs. 3–6. The samples are oriented with the downstream and upstream portions near the top and bottom of the images, respectively. The steps corresponding to the interface between the nickel nosetip and stainless steel forebody are located near the center of the images. The arrows are positioned to show the step as it passes through the region marked by the white ovals. The ovals demarcate the black marker marks, which were identified as a positions of interest and marked just after the molds had cured.

The surface impression molds taken at positions A, B, and F are relatively flat as a consequence of the BOLT II geometry, which generally made the molds easier to image. However, the black marker was more reflective than the black silicon-rubber mold material and did affect the step-height measurements for two samples as reported in the results section. The black marks were difficult to discern on most of the other samples. Samples taken on the gutter centerline (F) had an additional streamwise seam that represents the interface between the primary and secondary stainless steel forebody pieces. Molds from positions C and D had the most curvature and often needed to be rotated during acquisition to maximize the amount of data that could be measured. The rotated data were truncated following measurement to keep the width consistent with the other samples.

Molds were also made of the discrete "pizza-box" tripping elements on the secondary side of the model. Three molds were cast for each tripping element. The impressions from the centerline trip are pictured in Fig. 7. The arrow denotes the upstream-to-downstream orientation. Observation of the three sample images allows for distinguishing the true features from those created in the casting process. For example, the voids surrounding the impression, most notably on CL Trip (i), are not actually raised metal on the model because they are not present in all three castings. There are, however, some common features on the top surface of the tripping element. The circle from the thermocouple centered on the element is the most prominent.

A smaller trip was also located farther outboard on each side of the model. Samples of the element in quadrant 2 are pictured in Fig. 8. The arrow denotes the upstream-to-downstream orientation, and the two parallel diagonal lines on the casting resulted from tape covering the regions upstream and downstream of the trip to protect instrumentation. An impression from a thermocouple is observed centered approximately 2.0 mm upstream of the trip leading corner. The top surface of this tripping element is nearly smooth, with only light evidence of machining. Samples of the tripping element in quadrant 3 are pictured in three left images in Fig. 9. This element has thermocouples centered 2.0 mm upstream and inboard from the respective element corners. Two additional sensors are positioned 9.5 mm downstream of the tripping element lateral corners. A thermocouple is also on top of this tripping element, although there appears to be gaps around it. A higher resolution optical scan was also acquired, focusing in on the scratches near the inboard thermocouple for mold Q3 Trip (iii). This image is pictured on the right

of Fig. 9. Sanding was required to form the thermocouple junction, and efforts are made herein to characterize the size of the scratch marks.

2.2 Stylus

Measurements were also taken on the 20 interface-step samples using a stylus profilometer. Ten, 1-cm long profiles were made across the step on each sample, on or near the black marker marks. The measurements were independent of each other as the device was shifted after measuring each profile. The stylus tip was a 60-deg cone with a nominal 2 μm radius, and height data were collected every 0.5 μm that the stylus was traversed. The height values are resolved to 0.01 μm. The profilometer was calibrated prior to the measurements using a 2.970 μm arithmetic-mean-roughness precision reference specimen from the manufacturer. Stylus profilometer scans were also acquired on two different nosetip samples to compare with the surface roughness data obtained using the optical measurement device.

3 Methods of Analysis

3.1 Step Height

The location of the step was identified on most samples by a span of local maximum height values, which physically resulted from the silicon-rubber mold material filling a small $\mathcal{O}(100\ \mu\text{m})$ gap at the joint. Therefore, the step can be observed as a dividing line on most of the relative height maps shown in the results section. While the height maps provide a means for quick observation of the step direction, profiles must be extracted to more precisely determine the quantitative step height. The step height along the span for each sample was evaluated using the following process:

- Determine the spanwise bounds for evaluation. The sample should be relatively flat over the evaluation range.
- Analyze the streamwise profiles. For each spanwise position on each sample:
  - Determine the upstream and downstream locations, near the step, where the streamwise trend deviates. In practice, this was done by examining one streamwise profile for every 25 spanwise pixels. The streamwise locations for the remaining profiles were calculated through interpolation.
  - Determine lines of best fit from the upstream and downstream directions leading into the step. This was done by considering the 50 streamwise pixels outside the previously marked deviation pixels on each side of the step.
  - Extrapolate the lines of best fit to the streamwise step location. The relative height difference in the extrapolated lines at the step location is the step height.

The processing steps are summarized in Fig. 10 for sample Q3 E. Fig. 10(a) shows the relative height map of the sample. The white 'x' markers denote the

span to be evaluated where the surface is relatively flat. The evaluation span is longer for samples taken on the flatter regions of the model. The step is denoted by the white dashed line, where there is a clear discontinuity in relative height. Streamwise height profiles were evaluated at every spanwise pixel along the white line. PX 145 is a sample streamwise evaluation profile. It contains roughly 150 pixels (3.52 mm) on each sides of the step and is denoted by the solid blue line in Fig. 10(a). The measured heights along the profile were extracted from the height map and are shown in Fig. 10(b). The location on each side of the step where the incoming trend starts to change is denoted by a black 'x'. A best fit line (solid black line) from each of these points, directed away from the step, is generated using height values from the previous 50 pixels. The best fit lines are then extrapolated (dotted black lines) to the step location (dashed black line). The step height is the difference in relative height at the step location. Repeating this process over all spanwise pixels allows for the determination of step height in terms of spanwise distance. This plot is provided in the results section for each sample.

Each of the 20 samples was processed 10 times to moderate differences based on subjective evaluation. The choice of a linear fit, rather than a quadratic or some other fit, of the streamwise height data did affect the computed step-height values. Examination of different length and polynomial fits against the streamwise profiles revealed that a 50-point linear fit was most suitable. This evaluation component is regarded as the largest source of uncertainty in the step-height measurements.

Surface height profiles across the step of each mold were also acquired using a stylus profilometer. The profilometer scans were processed in a similar manner as the streamwise profiles obtained from the optical device, with the same physical distance (1.175 mm) comprising the linear fits. The purpose of the stylus measurements was to corroborate the values obtained using the optical device.

3.2 Other Features

The height values for the samples containing the tripping elements were each referenced to the area surrounding each respective element impression. The element footprints were evaluated by extracting linear profiles across the trips. The trip boundaries were set at approximately half of the trip impression depth. The height of each tripping element was computed in a similar manner as the step height, by finding the difference in relative height of the extrapolated best fit lines at the location of the boundary. This was done around the perimeter of the trip. Longer best-fit-line extrapolations were required in regions with casting defects.

Scratches and surface imperfections were analyzed by generating maps of relative surface height and extracting linear profiles through the features of interest.

4 Results

4.1 The Nosetip/Forebody Step

The height maps from the 20 step molds are presented in this section as well as the corresponding spanwise step-height profiles. The relative height values expressed

in these figures are scaled to each sample to highlight the salient features. The height maps allow for quick observation regarding the direction of the step, while the profiles allow for more precise quantitative observation. Note that an increase in height moving downstream across a step on the impression mold, herein expressed as a positive step height, corresponds to a backward-facing step on the actual BOLT II vehicle.

The relative surface height maps for samples taken in quadrant 1 are shown in Fig. 11. The relative flatness of samples Q1-4 A and Q1 B allowed for a tighter height scale and larger evaluation span. Sample Q1 D, taken from the leading edge, has the most curvature and, therefore, the narrowest evaluation span and some data voids. Height map Q1-4 A shows evidence of the black marker marks near the center span of the sample, particularly on the upstream side of the step. The height measurements are believed to be skewed to lower values due to the reflectivity of the marker and a relatively flat sample. A few other flat samples have similar artifacts, but only Q2 B shows a related skewing effect in the step-height profile and to a lesser magnitude. The step direction, either backward facing (B.F.) or forward facing (F.F.), with respect to the actual BOLT II vehicle is listed below the relative height map for each sample. The step directions are mixed in quadrant 1, with sample Q1 D being inconclusive (n/c).

The computed step-height profiles along the nose/forebody interface for samples in quadrant 1 are plotted in Fig. 12. The profiles are plotted for the span bounded by the white 'x' marks in the corresponding height maps (Fig. 11). The small black ovals correspond to the positions of interest from Fig. 3. The black arrows indicate the position of the span segment with respect to nearby quadrants or features. A positive relative height value is associated with a backward-facing step on the actually BOLT II vehicle. Most of the samples show considerable variation in step height along the span. Gradients are consistently higher for samples C–E, which were acquired near the leading edge. The step-height profile for Q1-4 A appears to be the most constant aside from the spanwise position between 8–10 mm, which corresponds to the location of the marker. The backward-facing step height appears to be artificially increased by roughly 15 μm due to the black marker marks on this particular sample. Samples Q1 B and Q1 C suggest a forward-facing step of generally less than 30 μm. Sample Q1 D indicates a large step-height variation across its limited span. The step-height value starts out highly positive, meaning the model has a backward-facing step on the gutter side of the leading edge. The step direction changes and becomes forward-facing on the centerline side. Location Q1 E also has a large variation but is highly backward-facing, with magnitudes over 100 μm for part of the sample span.

The relative surface height maps for samples acquired on the secondary side in quadrant 2 are shown in Fig. 13. Sample Q1-2 F was taken in the center of the gutter, so it not only has the nosetip/forebody interface step but also includes the seam from the mating of the primary and secondary forebody surfaces. The vertical maroon band signals that there is a gap between the forebody surfaces that is deeper and more expansive than any observed between the nose and forebody. The step height does not appear to vary much between the nose and forebody across the forebody junction. There were data voids again for sample D, but it was measured

in the same orientation as the others in quadrant 2. The Q2 B height map contains artifacts due to the black marker.

The computed step-height profiles along the span for samples in quadrant 2 are plotted in Fig. 14. The samples indicate definitive backward-facing steps within the gutter (E and F), small backward-facing steps on the experimental surface near the leading edge (C and D), and a small forward-facing near the centerline (B). Gutter sample Q1-2 F registered the largest step at 195 μm due to the $\mathcal{O}(300\ \mu\text{m})$ wide gap between the forebody pieces at the nose interface. Otherwise, the backward-facing step on that sample was near 60 μm for both forebody pieces. The same magnitude is observed on the gutter side of sample Q2 E but decreases to near zero on the leading-edge side of the sample. The step at Q2 B is roughly 10 μm, and the black marker influenced part of the sample span by about 5 μm, which is considerably less than for Q1-4 A.

The relative surface height maps for samples in quadrant 3 are shown in Fig. 15. Samples Q2-3 A, Q3 B, and Q3 C appear to have moderate forward-facing steps across the span. The step direction reverses in the gutter. Sample Q3 D still has some data voids despite being measured at a 90-deg rotation. The corresponding step-height spanwise profiles for samples in quadrant 3 are shown in Fig. 16. The samples indicate that the largest forward-facing steps on the experimental surface are in this quadrant, with values ranging from 40–60 μm near the centerline (Q2-3 A and Q3 B) and just below 40 μm on the centerline side of Q3 C. The highest absolute step-height value that was measured on the nose interface seam is the near 120 μm backward-facing step in Q3 E that resulted from a continuation of the large gradient observed on the leading-edge sample Q3 D.

The relative surface height maps for samples in quadrant 4 are shown in Fig. 17. The magnitude of the streamwise step at location F and the gap between the forebody pieces is less on this side of the model in comparison to location Q1-2 F. Two samples had to be rotated for data acquisition in quadrant 4, and there were again considerable data voids for the highly-curved leading-edge sample, Q4 D. The height map for Q4 B demonstrates a backward-facing step for the full span. The calculated step-height values across the span of samples within quadrant 4 are shown in Fig. 18. The step at the gutter is small in magnitude and varies in direction. The step direction changes from forward to backward facing around the leading edge to the primary experimental surface. A moderate 40–65 μm backward-facing step exists near the centerline at Q4 B but is back to near zero at the centerline Q1-4 A.

The direction and magnitude of the step height for all samples is summarized in Table 2. The tallest step averaged over a 20-pixel (0.47-mm) span is recorded for the optical measurements as is the mean step height at the marker. Profiles were also acquired using the stylus profilometer near the marker, and those mean height values are listed for comparison. The values are generally in good agreement. The largest differences are observed for samples with large gradients in step height across the span, where a significant difference could be observed depending on where measurements were made in relation to the marker. The stylus corroborates the notion that the black marker marks skewed the optical measurements on samples Q1-4 A and Q2 B since each stylus-measured step height is close to its respective optically-measured height just outside of the marker.

4.2 Tripping Elements

The largest tripping element was on the centerline of the secondary experimental surface. The measured side-to-side distances for the three centerline trip samples were 7.92 ±0.09 mm at 50% height of the element. This is equivalent to the side length of the square-planform element. Height maps for all three centerline trip molds are shown in Figs. 19(a–c). The white arrow in Fig. 19(a) indicates the approximate flow direction. Casting defects that resulted in some divots around the perimeter of the trip impression are observed in Fig. 19(a). A faint circle is noted at the center of the tripping element for all three molds. This indicates that the thermocouple is slightly recessed with respect to the top of the trip. Select profiles were extracted from the sample CL Trip (ii) height map and are plotted in Fig. 19(d). The colors of the lines drawn on the height map correspond to the colors of the profiles in Fig. 19(d). The physical directionality of the profiles is left to right or top to bottom with respect to the height map. The profiles show strong overlap, representing a consistent height across the tripping element. The thermocouple, which has a maximum recession of less than 100 μm causes the most prominent deviation in profile PX390 (black) from the others.

The leading-edge trips in quadrants 2 and 3 are nominally the same size and had measured side-to-side distances of 2.73 ±0.05 mm. Height maps for all three Q2 leading-edge trip molds are shown in Figs. 20(a–c). The height map from sample Q2 Trip (ii) was chosen for profile extraction since that mold was free from defects around the edge of the trip impression. Again, the profiles plotted in Fig. 20(d) are quite similar, but there is some variation in slope at the top of the element. This means that the trip height with respect to the surface is slightly different on different sides of the element. The height values will be examined in more detail later in this section. Height maps for all three Q3 leading-edge trip molds are shown in Figs. 21(a–c). Comparisons between the molds indicate that the divots around the trip impressions are casting defects and are not actually present on the BOLT II model. The height maps from all samples show that the installed thermocouple is recessed from the top of the trip. The height map from sample Q3 Trip (i) was chosen for extracting the profiles across the trip impression. Profiles PX420 (black) and PX545 (orange) are not influenced by the thermocouple since they run near the edges of the trip. The other two profiles run through the largest extreme, physically representing a gap between the thermocouple and the trip surface.

Further analysis was done to characterize the trip height along the edges of each tripping element. The samples chosen previously in Figs. 19–21 for profile extraction were used again to analyze the height of each trip along the edges. Figure 22(a) defines the sides of each tripping element and the direction of the profiles. Figures 22(b)–(d) plots the trip height along the edges of each respective trip in the direction indicated by the diagram in (a). The trip heights are fairly constant for each trip with respect to the different edges and the position along those edges. The measurements generally corroborate the Q2 and Q3 trips as being the same size, but the Q3 trip shows more variation. The trip heights along the edges are summarized in Table 3. Values listed in the table are mean height values (in μm) over the central 80% length of each edge. The centerline trip height measured in at

2623 ±12 μm, while the leading edge, quadrant 2 and 3, trip heights were 897 ±5 μm and 891 ±18 μm, respectively.

4.3 Other Features

This subsection examines irregularities on the model surface, most notably indentations that likely resulted from particle impact during a prior ground test and surface roughness due to machining and thermocouple installation.

4.3.1 Nosetip

Two impression molds were cast of the nosetip, one consisting of only the leading edge and one with the nosetip and a portion of the upstream secondary experimental surface. The nosetip leading-edge sample is pictured twice in Fig. 23 due to the amount of curvature and glare off the sample. It was tilted to allow for better observation of defects toward the secondary side in Fig. 23(a), and tilted the other way to see those toward the primary side in Fig. 23(b). The most prominent features on the mold are small raised bumps, which correspond to pitting on the actual flight model. All of the indentations are relatively small, with a maximum depth of 20 μm.

The small bumps can be observed more clearly on the mold that contains part of the secondary side of the nosetip shown in Fig. 24. The sample was tilted in different directions in Figs. 24 (a) and (b) to allow for more features to be observed. The secondary side is the side with less curvature at the top of the images. A string of surface bumps visible in Fig. 24(b) is bracketed in red. The largest is above the center of the bracket and corresponds to a hit with a depth of 33 μm. The maximum depth of all other defects is 20 μm.

4.3.2 Primary Side

Some divots or pitting were noted at the nosetip leading-edge corner in quadrant 1. The mold at that location was imaged and is pictured on the left side of Fig. 25. Three different images of the same mold were acquired due to the curvature of the sample. The locations of the smaller optical images with respect to the primary image are boxed in the primary image. More features appear when the sample is tilted optimally. Flow is from bottom to top in the images. Three of the largest features are identified and numbered (i)–(iii). Height maps are shown referencing a zero height to each feature. The height of each bump on the mold was estimated by extracting profiles across the defect and removing a best-fit quadratic from the original profile. The most outboard feature (i) had a maximum height of about 60 μm and distance across of 570 μm. Feature (ii) was smaller with a maximum height of about 32 μm and was 440 μm across. Feature (iii) had the largest footprint at 650 μm across, but the maximum height was less than (i) at about 51 μm.

This same sample taken near the nosetip and leading edge in quadrant 1 was further analyzed for surface roughness. Distinct, parallel, spanwise-directed machining lines were observed on the flat portion of the sample corresponding to the

face of Q1. Figure 26(a) shows an image of the sample with increased magnification. Flow is from bottom to top and the blue line is sketched in the streamwise direction. The surface height profile represented by the blue line is shown in Fig. 26(b). There is relatively little height change over the 4.48 mm profile, with the relative height bounded by ± 4 μm, but there is clearly some periodicity. The same profile was further analyzed for surface roughness. A shortpass filter ($\lambda_c = 0.8$ mm) was implemented to separate the roughness from the waviness. The power spectral density and arithmetic-mean (Ra) and root-mean-square (Rq) roughness values were calculated for the resulting profile. These calculations were repeated for and averaged over the 710 adjacent profiles over the area shaded in blue in Fig. 26(a). The resulting surface roughness height values were Ra = 1.08 μm and Rq = 1.28 μm. The roughness spectrum in Fig. 26(c) shows a strong peak at a wavelength of 176 μm and at the first harmonic. The other values across the spectrum are quite low in comparison.

Twenty 6-mm scans of the same sample were made in the same direction and general area using the stylus profilometer. The profiles were reduced into 5-mm evaluation lengths and 2.5-mm sample lengths. Although the sampling lengths differed between the measurement techniques, the roughness parameters should be comparable since those are based on the profiles after the shortpass filter. The resulting roughness parameters with the stylus were slightly lower than those obtained using the optical device, with Ra = 0.94 μm and Rq = 1.12 μm. The spectra show remarkable agreement. The primary spectral peak is at 179 μm, meaning the difference between the stylus and optical primary peaks is within the wavelength resolution.

4.3.3 Secondary Side

Quadrant 3 has a quasistreamwise-directed line of three divots along the nose that are believed to be the result of impacts from the same particle due to similar depths and footprints of the damage. The most upstream divot is at the leading-edge corner as circled in the photograph of Fig. 27(a). The impression mold is pictured in Fig. 27(b) with the flow from bottom to top. A relative height map in μm of the mold, with the height referenced around the defect, is pictured in Fig. 27(c). The bump on the mold corresponds to a gouge that is 50 μm deep, 0.8 mm wide, and extends 2.0 mm in the streamwise direction on the actual BOLT II model.

A surface impression was not taken on the second divot in the line of Q3 impacts but was made on the third divot, which was also surrounded by a couple smaller pits. That cluster is circled in Fig. 28(a), which shows the position of the defects in relation to the model. The resulting mold, mirrored about the streamwise axis, is shown in Fig. 28(b) with profiles drawn across the three notable features. A map of relative surface height in μm is shown in Fig. 28(c). The profiles corresponding to the lines drawn in Fig. 28(b) are shown in Fig. 29(a). The largest defect on the model, farthest outboard toward the leading edge, has a maximum depth of 46 μm with a roughly 2.6 x 1.0 mm footprint. The other two depressions are smaller and more shallow with depths of 10 μm and 17 μm. The surface roughness was also evaluated using profiles extracted in the same direction as those plotted in Fig. 29(a) but not passing over the aforementioned defects. The profiles were 24.1 mm

long, and a cutoff wavelength of 0.8 mm was applied to isolate the roughness from the waviness. The spectrum plotted in Fig. 29(b) is the result of 450 averages. The wavelength, again, has a sharp peak at 176 μm; however, the content is broader than it was farther upstream on the nose in Q1. The average roughness for the Q3 profiles is Ra = 1.24 μm and Rq = 1.94 μm. Eleven 12.5-mm stylus measurements were also made in similar areas of the sample. The evaluation length was kept at 12.5 mm, and the sampling length was set at 2.5 mm, with the same shortpass filter of 0.8 mm. The stylus PSD is also plotted in Fig. 29(c). Though the agreement across the spectrum is not as good as it was for Q1, the primary spectral peak is identified using both measurement methods. The stylus roughness parameters are also lower at Ra = 0.63 μm and Rq = 0.89 μm. The reason for the discrepancy is currently unclear. The measurements were repeated using both devices, and the optical measurements were also performed using the high-magnification lens, yielding similar results to those in Fig. 29(c).

The scratch marks used to activate the thermocouple on the forebody near the tripping element in quadrant 3 were also examined. The same zoomed in image from Fig. 9 is also pictured in Fig. 30(a) with lines representing the locations where height profiles were extracted. Those profiles are shown in Fig. 30(b). Profile (i) goes through the roughest sanding and has several peak-to-valley heights at or above 5 μm. Profile (ii) goes through a region where the scratches are coming to an end and are roughly half as deep as for (i). Profile (iii) is outside of the thermocouple sanding region and demonstrates the lowest surface roughness.

5 Conclusions

Surface impression molds were cast prior to the BOLT II flight test to preserve surface flaws for later analysis that is provided herein. Measurements were taken on the silicon-rubber samples using optical and contact devices. An algorithm was developed to compute the step height at 20 different positions around the perimeter of the nosetip/forebody interface. The step varied in magnitude and direction, but all values obtained on the experimental surfaces using both measurement devices were found to be below 100 μm. The heights of the centerline and leading-edge trips on the secondary side of the model were calculated using a similar approach with optical scans of the samples. Finally, defects believed to be from particle impacts were evaluated for depth and footprint, and surface roughness parameters and spectra were computed at a couple of locations on the nosetip.

References

1. Kostak-Teplicek, H. E., "Stability and Breakdown Measurements on the AFRL/AFOSR Boundary Layer Turbulence (BOLT II) Flight Geometry," Ph.D. Dissertation, Texas A&M Univ., College Station, TX, 2022.

2. Johnston, Z. M., Hemati, M. S., and Candler, G. V., "Modal Analysis of Instabilities in the BoLT-2 Flowfield," AIAA SciTech Forum, AIAA Paper 2022-0348, 2022. https://doi.org/10.2514/6.2022-0348.

Table 1: Relative position of molds within each quadrant.

Letter	Location Description
A	Experimental centerline
B	2” off centerline
C	Exp. to LE merger
D	Leading edge
E	LE to gutter merger
F	Gutter centerline

Table 2: Estimated nosetip/forebody step height values (μm).

Sample	Step Direction on BOLT II	Largest (optical)	At Marker (optical)	At Marker (stylus)
Q1-4 A	B.F.	21.6*	20.9*	0.4
Q1 B	F.F.	31.7	28.1	19.8
Q1 C	F.F.	27.1	9.2	8.3
Q1 D	n/c	74.5 (B.F.)	10.7 (B.F.)	37.4 (B.F.)
Q1 E	B.F.	109.7	66.2	71.0
Q1-2 F	B.F.	n/a	n/a	n/a
Q2 E	B.F.	69.1	23.9	33.8
Q2 D	n/c	11.0 (B.F.)	8.8 (B.F.)	1.7 (B.F.)
Q2 C	B.F.	18.4	4.8	5.2
Q2 B	F.F.	17.6	4.1*	8.0
Q2-3 A	F.F.	56.0	41.0	33.5
Q3 B	F.F.	64.1	52.1	49.6
Q3 C	F.F.	85.1	51.1	67.3
Q3 D	F.F.	50.9	21.2	23.1
Q3 E	B.F.	115.8	77.6	47.7
Q3-4 F	n/c	n/a	n/a	n/a
Q4 E	F.F.	53.2	41.2	48.1
Q4 D	F.F.	51.5	11.0	5.0
Q4 C	B.F.	63.7	57.0	61.1
Q4 B	B.F.	66.4	55.5	40.5

B.F.=backward facing, F.F.=forward facing
n/c=inconclusive, n/a=not applicable, *=marker influenced

Table 3: Estimated trip heights (μm). These are mean height values along the central 80% length of each side.

Sample	ht1	ht2	ht3	ht4
CL Trip (i)	2622	2621	2620	2634
CL Trip (ii)	2618	2621	2620	2633
CL Trip (iii)	2614	2611	2623	2625
Q2 Trip (i)	896.0	896.3	894.9	898.5
Q2 Trip (ii)	900.1	892.6	891.7	902.4
Q2 Trip (iii)	901.8	897.6	893.3	898.9
Q3 Trip (i)	893.0	878.7	893.2	909.4
Q3 Trip (ii)	881.2	872.9	909.1	904.4
Q3 Trip (iii)	895.2	873.4	894.0	906.0

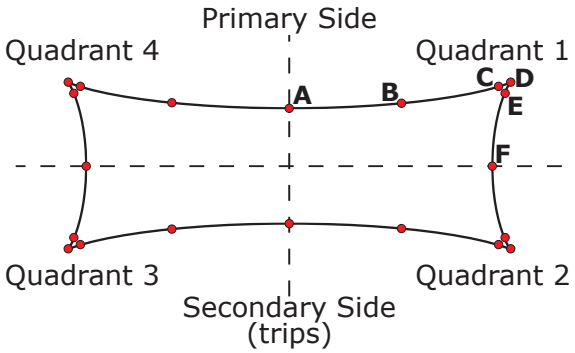

Figure 1: Schematic of the BOLT II nosetip/forebody mating plane. Quadrants 1–4 are defined, and the relative positions A–F are denoted within Q1. The perspective is looking downstream from the nosetip.

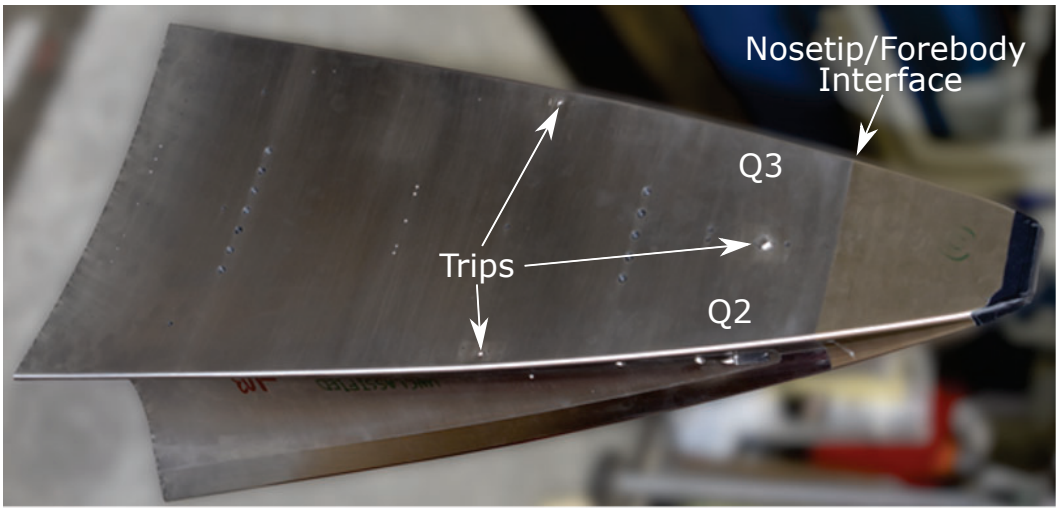

Figure 2: A photograph of the BOLT II model with the secondary side up. The locations of tripping elements are marked along with the nosetip/forebody interface [Photo: NASA].

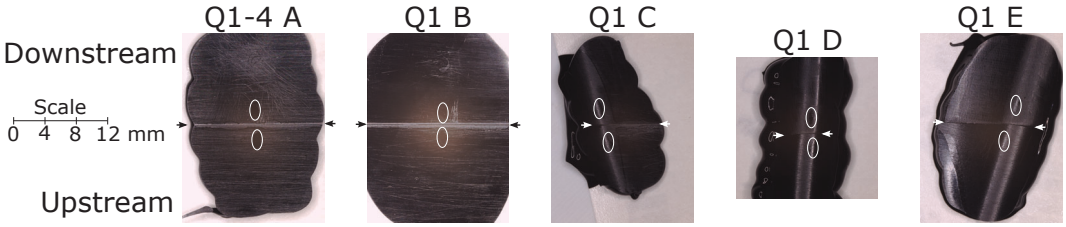

Figure 3: Images of nosetip/forebody interface step samples from locations in quadrant 1. The arrows in each image denote the location of the step relative to the region of interest. The region of interest is marked with black marker on each sample, which is circled in the figure for clarity.

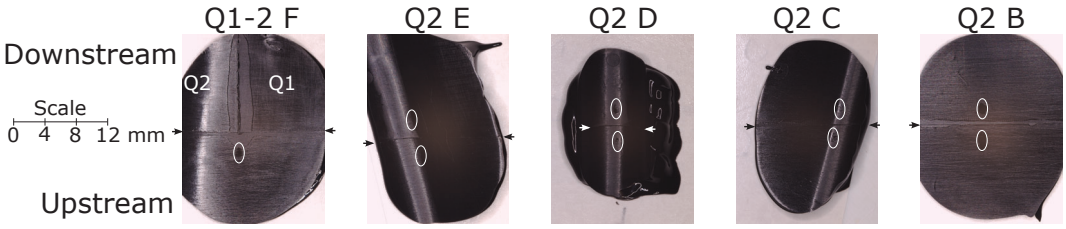

Figure 4: Images of nosetip/forebody interface step samples in Q2.

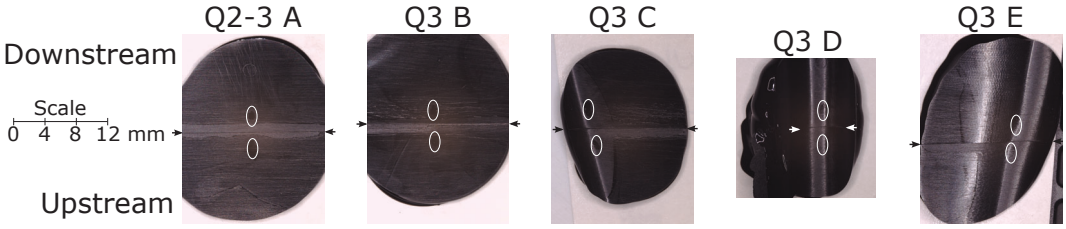

Figure 5: Images of nosetip/forebody interface step samples in Q3.

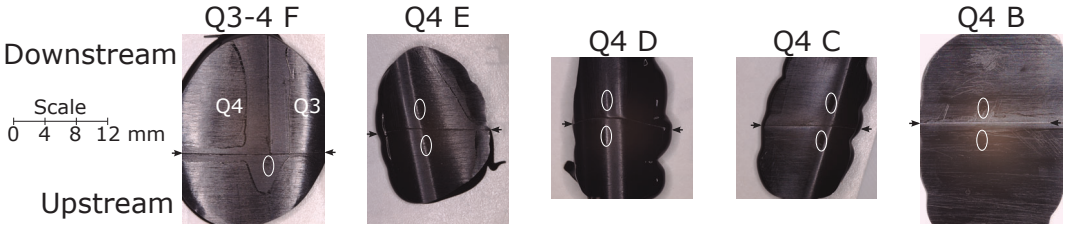

Figure 6: Images of nosetip/forebody interface step samples in Q4.

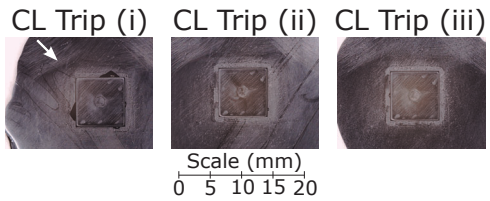

Figure 7: Images of the centerline trip mold samples. The arrow indicates the flow direction.

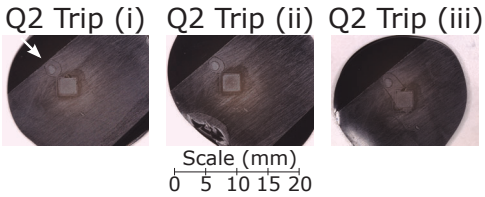

Figure 8: Images of the Q2 trip mold samples. The arrow indicates the flow direction.

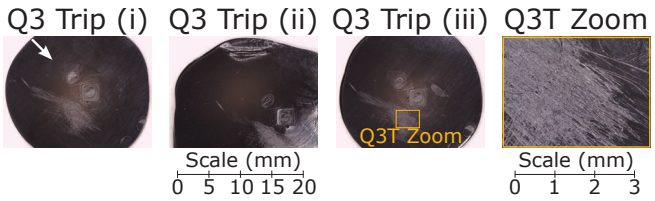

Figure 9: Images of the Q3 trip mold samples are in the three images on the left. The arrow indicates the flow direction. A magnified portion of Q3 Trip (iii) is shown in the right image to highlight the roughness near the thermocouple.

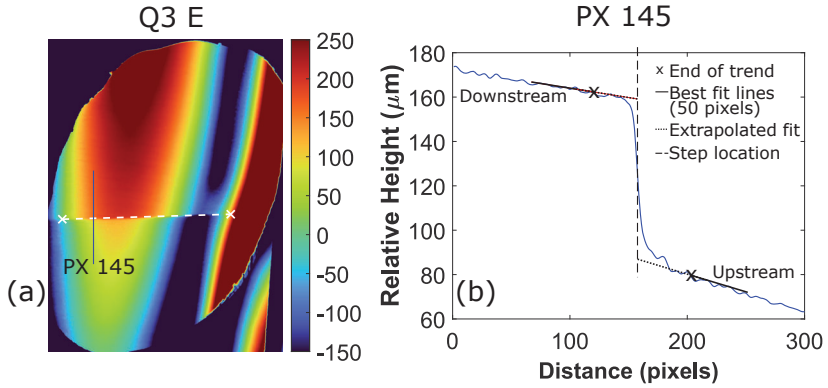

Figure 10: Process to determine the step height. (a) A representative surface height map. The evaluation span is bounded by the white 'x' markers, and the white dashed line overlays the step. The solid blue line represents a streamwise profile at location PX 145. (b) The relative height of profile PX145. The black 'x' markers represent where the trend incoming to the step begins to diverge. The solid black lines are the best fit lines for the incoming trends. The dotted black lines are the extrapolations of the best fit lines to the step location (dashed black line).

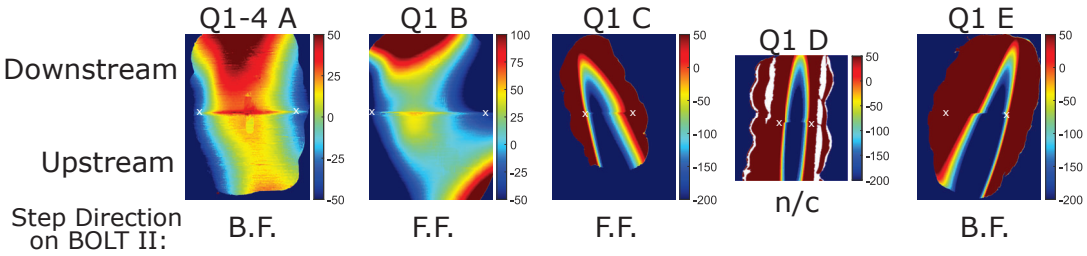

Figure 11: Maps of relative surface height (μm) for step samples in quadrant 1. The color bar scales differ between maps to highlight the salient features. The heights are referenced to an area just upstream of the step. Flow is from bottom to top. The white 'x' markers bound the evaluation span where the sample was relatively flat. The step direction on the actual BOLT II model is indicated below each height map.

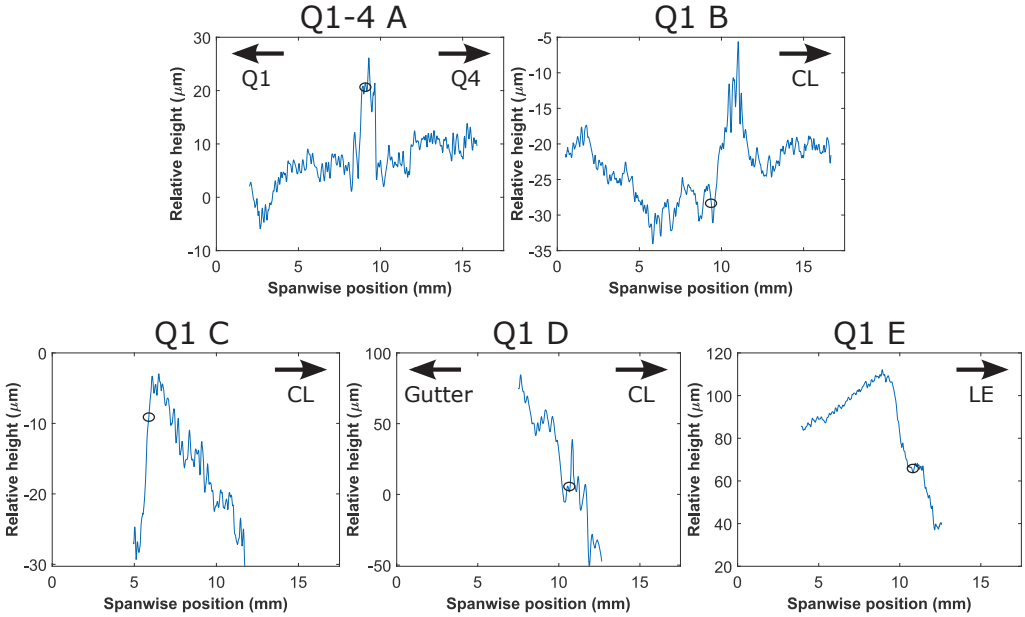

Figure 12: Measurements of step height along the span for samples in quadrant 1. The black ovals are the positions of interest based on the black marker marks. Positive values represent backward-facing steps on the actual flight vehicle.

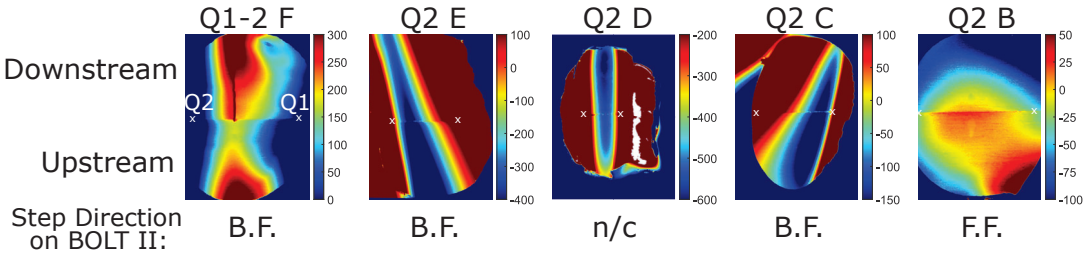

Figure 13: Maps of relative surface height (μm) for steps in Q2.

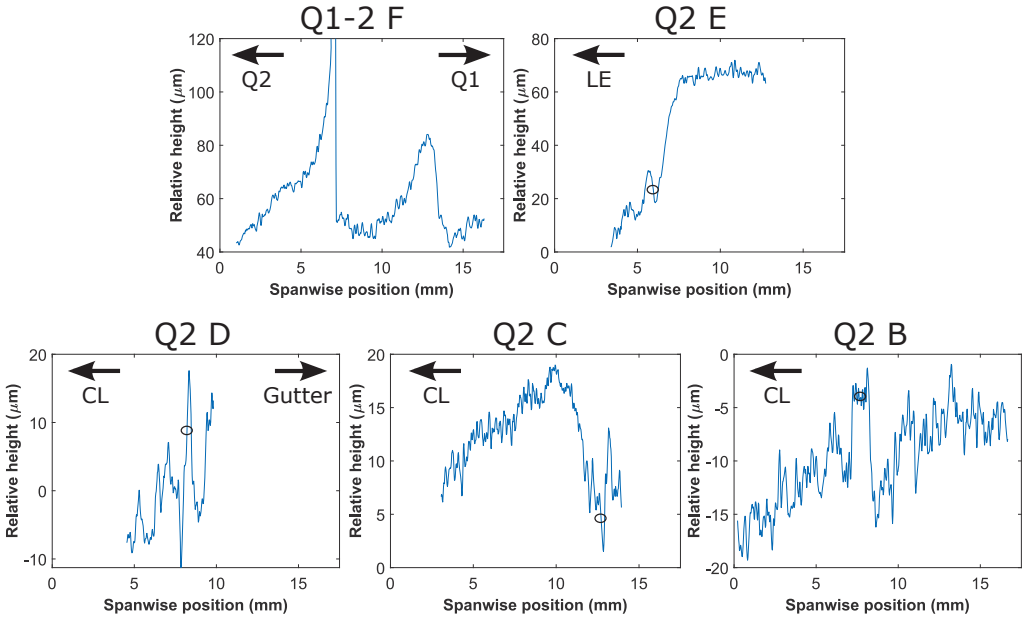

Figure 14: Measurements of step height along the span for samples in Q2. Positive values represent backward-facing steps on the actual flight vehicle.

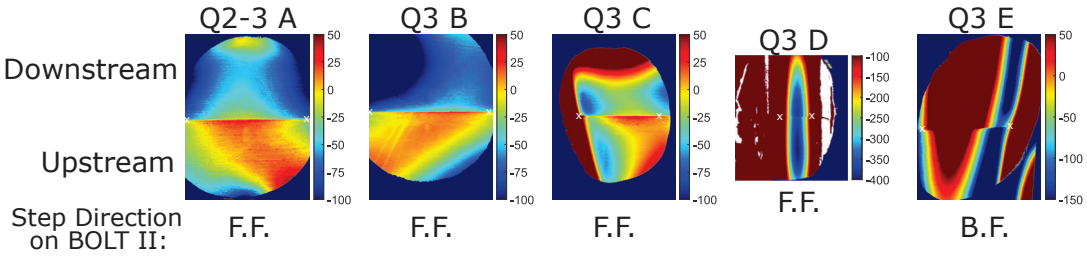

Figure 15: Maps of relative surface height (μm) for steps in Q3.

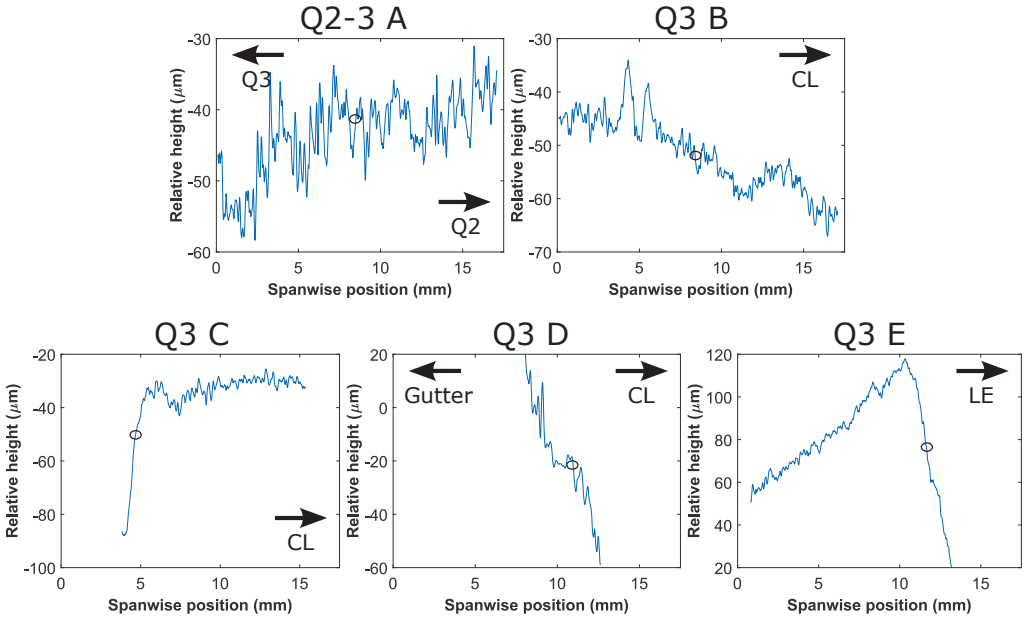

Figure 16: Measurements of step height along the span for samples in Q3. Positive values represent backward-facing steps on the actual flight vehicle.

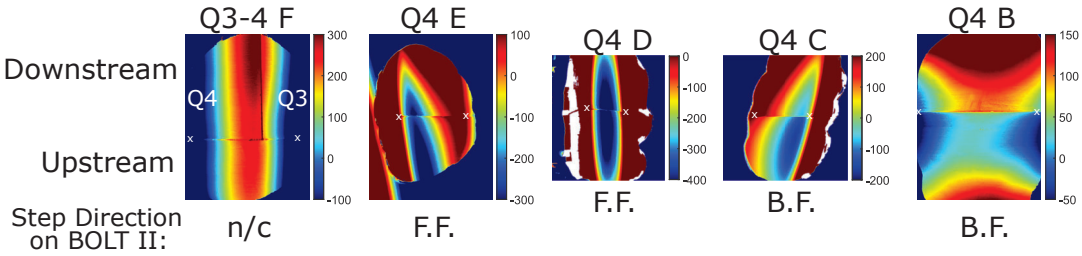

Figure 17: Maps of relative surface height (μm) for steps in Q4.

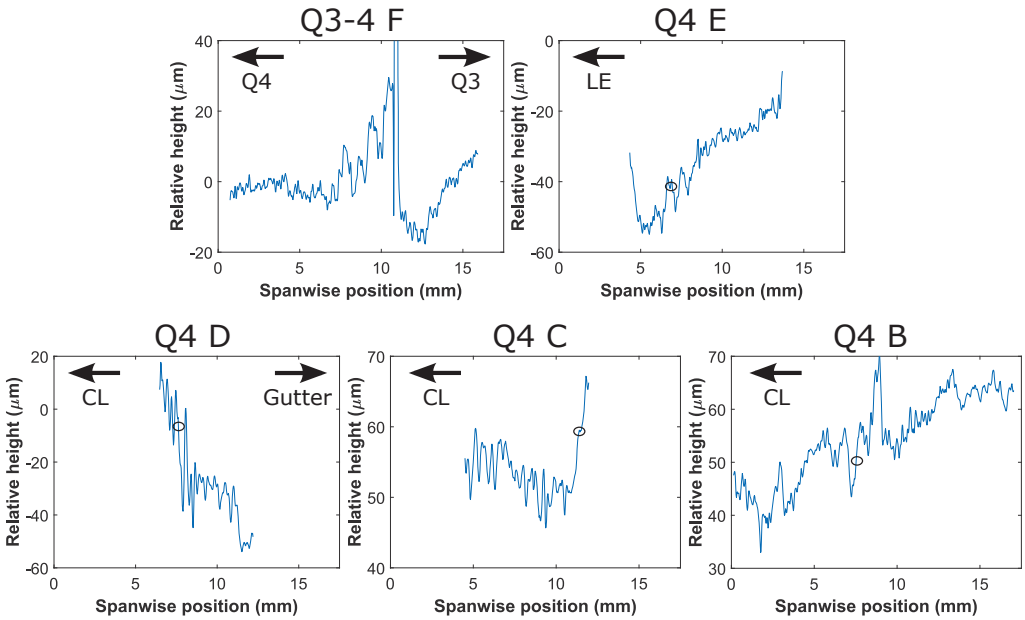

Figure 18: Measurements of step height along the span for samples in Q4. Positive values represent backward-facing steps on the actual flight vehicle.

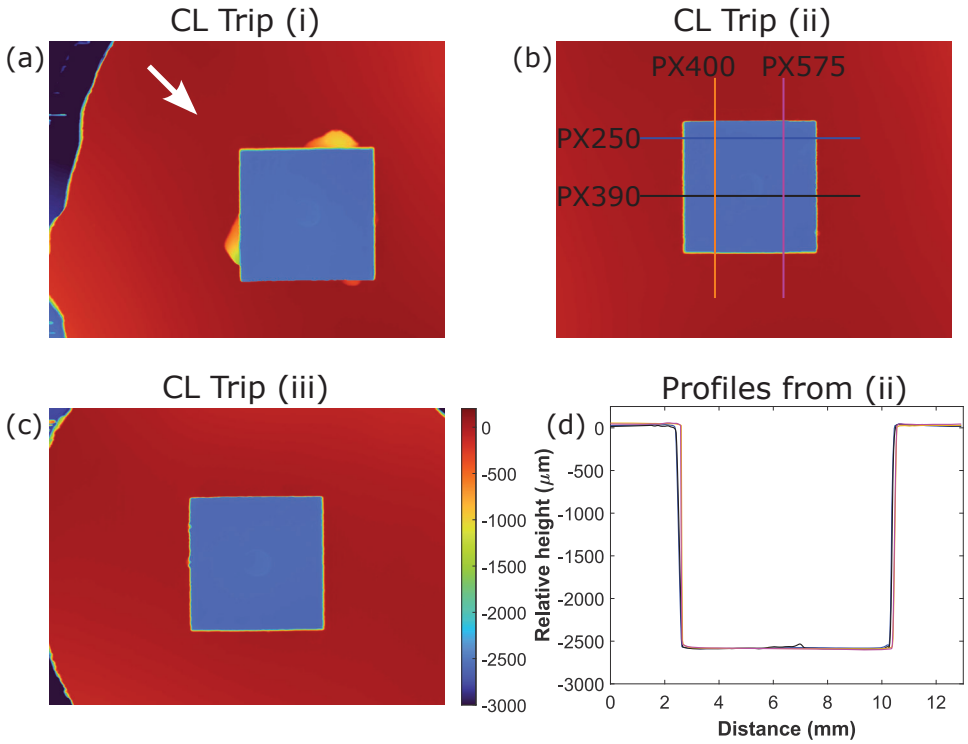

Figure 19: The centerline tripping element. (a)–(c) are height maps of the three impression molds obtained for this trip. The arrow in (a) shows the flow direction. Profiles from (b) were extracted and are plotted in (d).

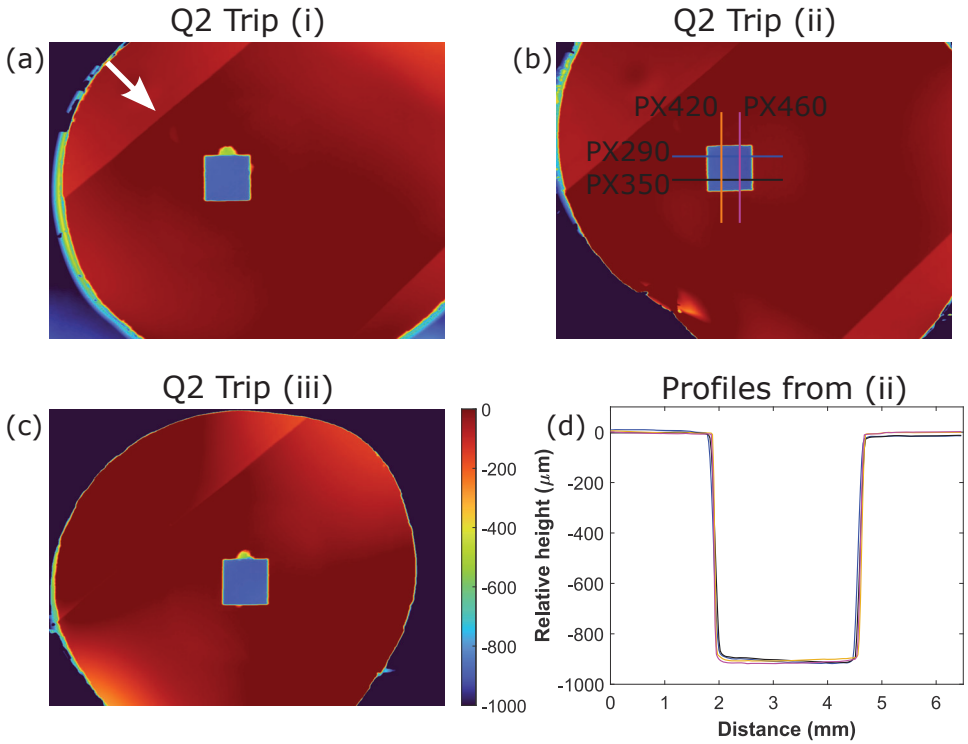

Figure 20: The tripping element located near the leading edge in quadrant 2.

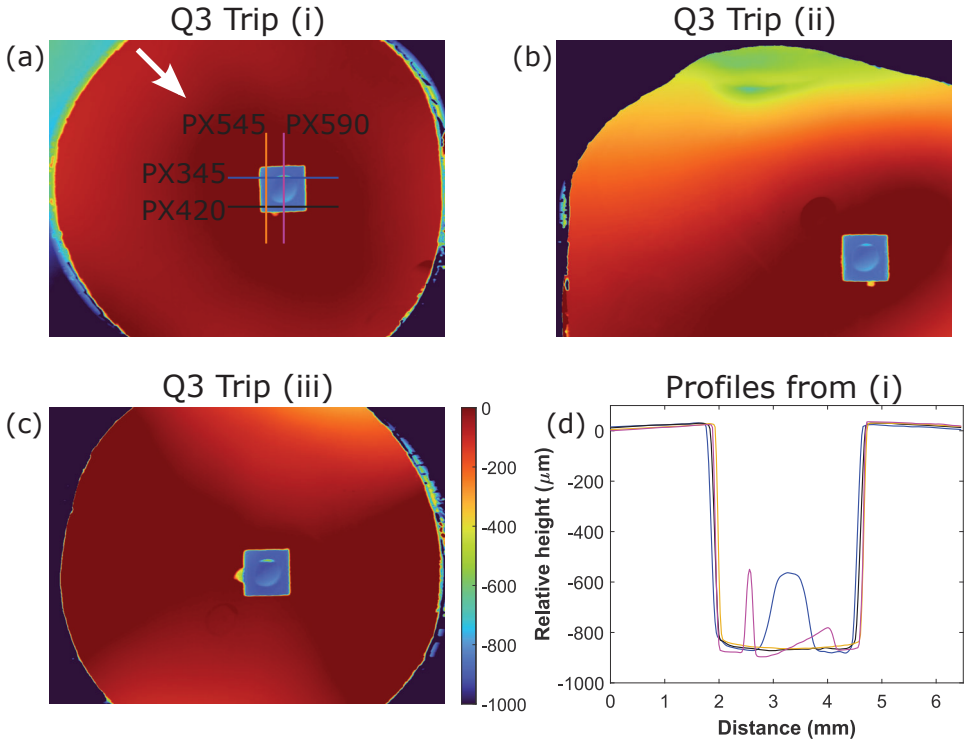

Figure 21: The tripping element located near the leading edge in quadrant 3.

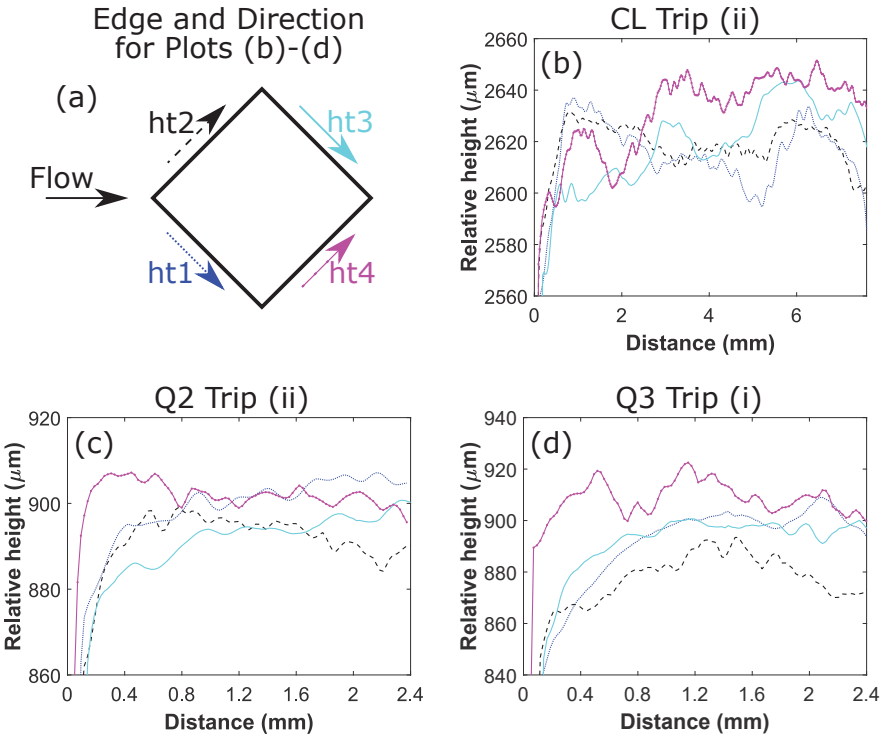

Figure 22: Evolution of step height along the edges of the trips. (a) Diagram of a tripping element with the edges defined. (b)–(d) Height profiles of the three trips (CL, Q2, Q3) as determined along the four edges, matching line colors and styles from (a).

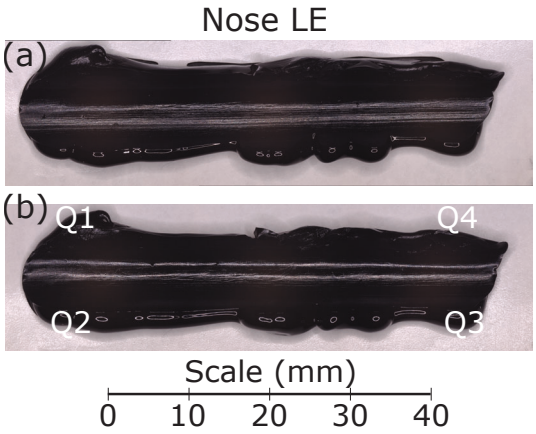

Figure 23: Photographs of the nosetip impression mold. (a) The mold is tilted to observe defects toward the secondary side, and (b) the mold is tilted to see defects on the primary side. The quadrant positions downstream of the tip are given for reference.

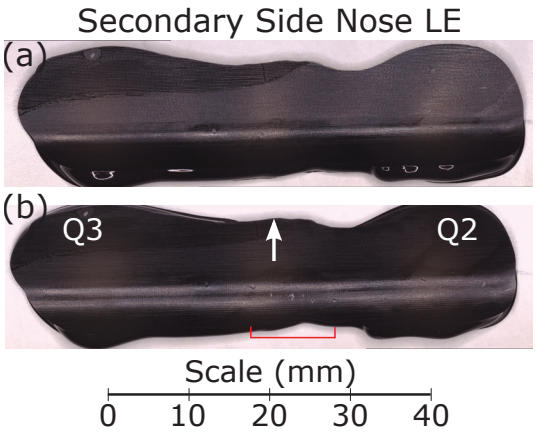

Figure 24: Photograph of a second nosetip mold that includes part of the secondary side of the nosetip. The mold is tilted in different directions in (a) and (b) to observe the defects. The flow direction and quadrants are given on the secondary side in (b). The red bracket bounds the highest concentration of defects.

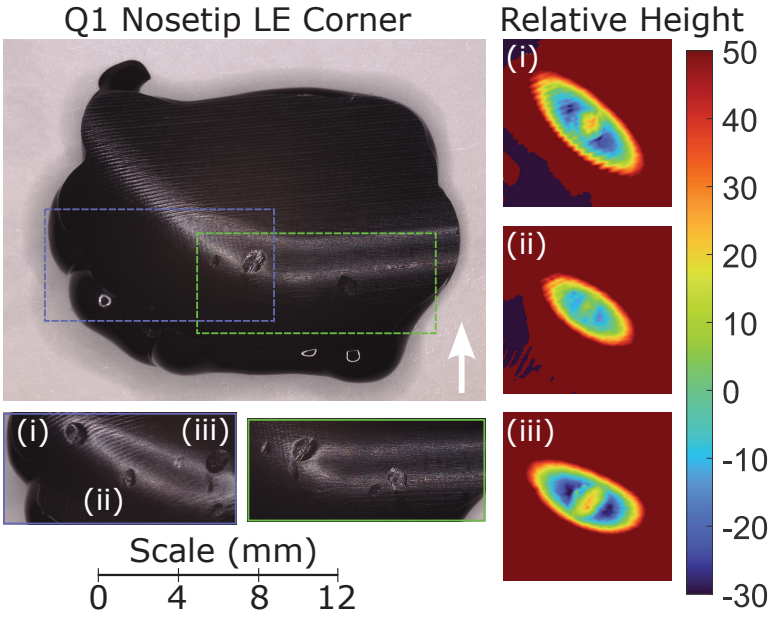

Figure 25: Defects in quadrant 1 near the leading edge and nosetip. Photographs of the mold are pictured on the left, with the smaller images showing regions that were measured with the sample at different tilt. Flow is from bottom to top in all images. Defects (i)–(iii) were identified as the most prominent, and height maps for each are given on the right. The height, in μm, is referenced to an area around each respective defect.

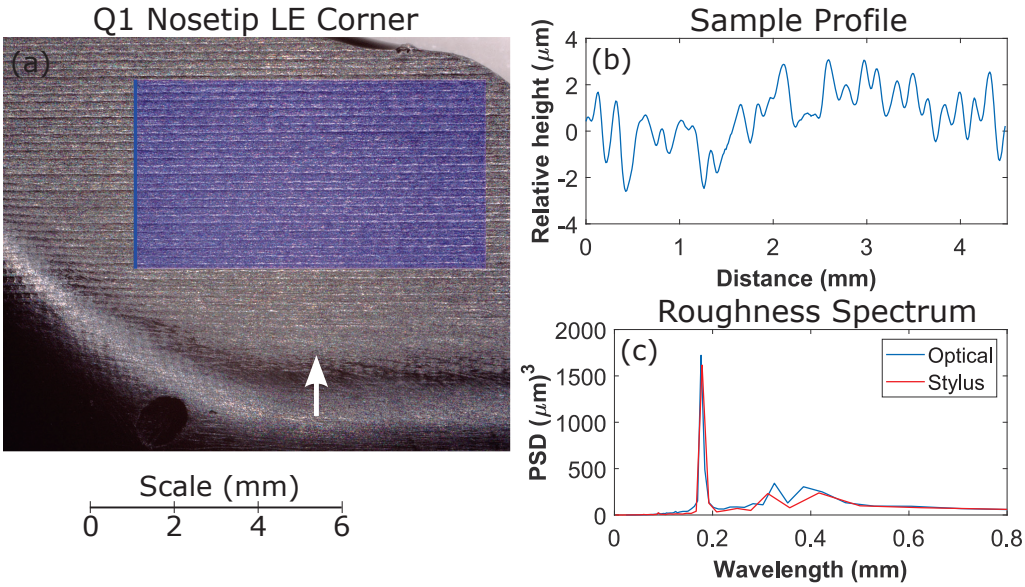

Figure 26: Surface roughness in quadrant 1 near the leading edge and nosetip. (a) A photograph of the same sample as Fig. 25 but at a higher magnification. Flow is from bottom to top. The solid blue vertical line defines a streamwise profile; the height values along which are plotted in (b). The average PSD of this profile and all adjacent profiles bounded by the area of the box in (a) is given in (c). The same plot also shows a comparison PSD obtained from stylus measurements in the same region of the sample.

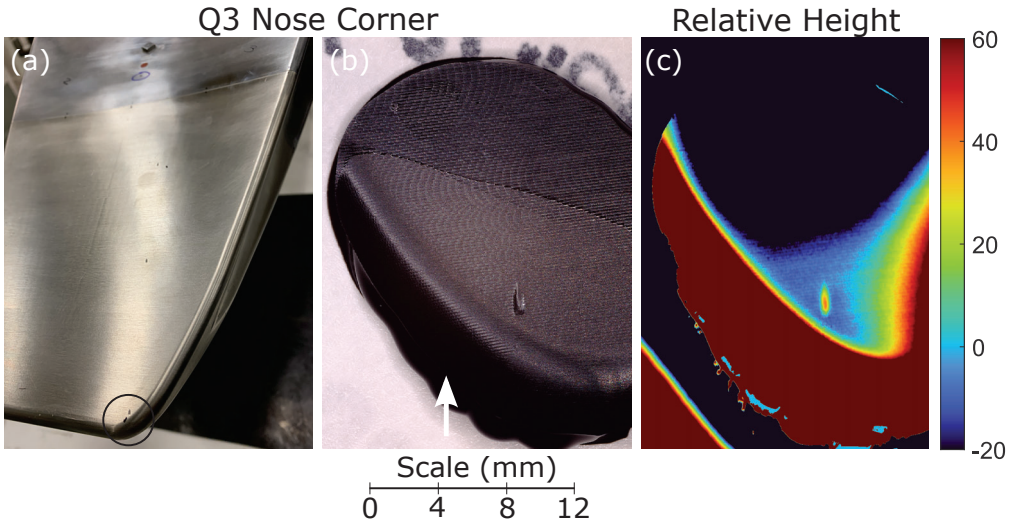

Figure 27: A defect in quadrant 3 near the leading edge and nosetip. (a) A photograph showing the location of the defect with respect to the larger model. (b) The impression mold of the defect and (c) A height map (μm), referenced to the height around the defect.

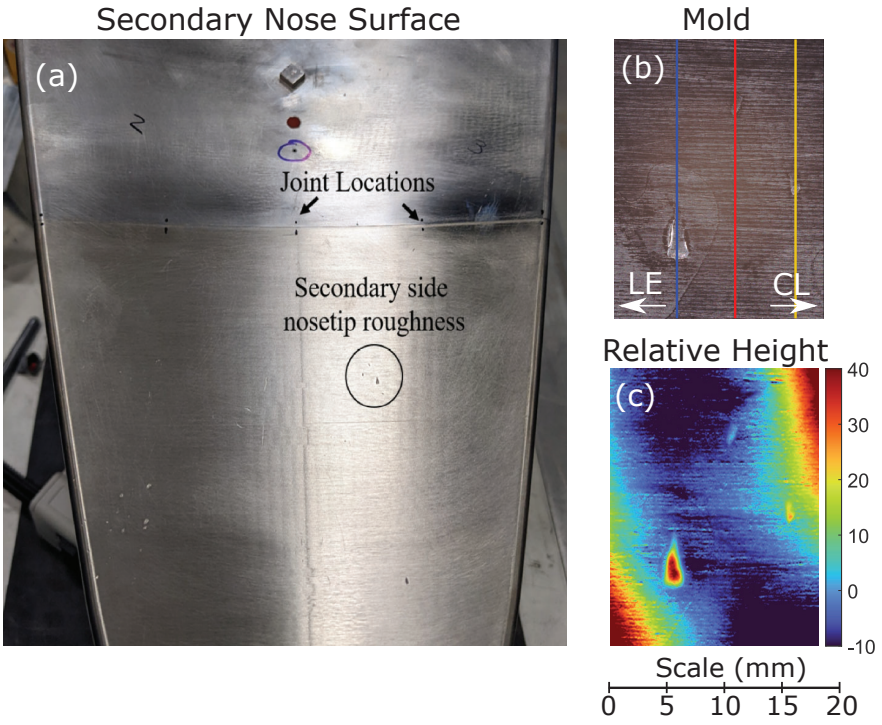

Figure 28: A cluster of defects in quadrant 3 on the nosetip. (a) A photograph showing the location of the cluster in relation to the larger model. (b) The impression mold with profiles defined for consideration. (c) A height map (μm) of the mold, where the average height was set as the reference.

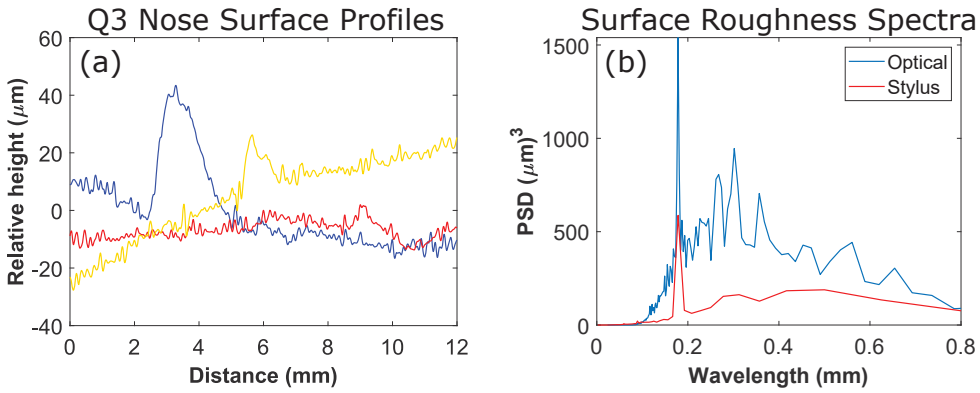

Figure 29: Further analysis of the sample presented in Fig. 28. (a) Height profiles in the streamwise direction as defined in Fig. 28(b). (b) The PSDs obtained from averaging streamwise profiles that did not pass through the defects.

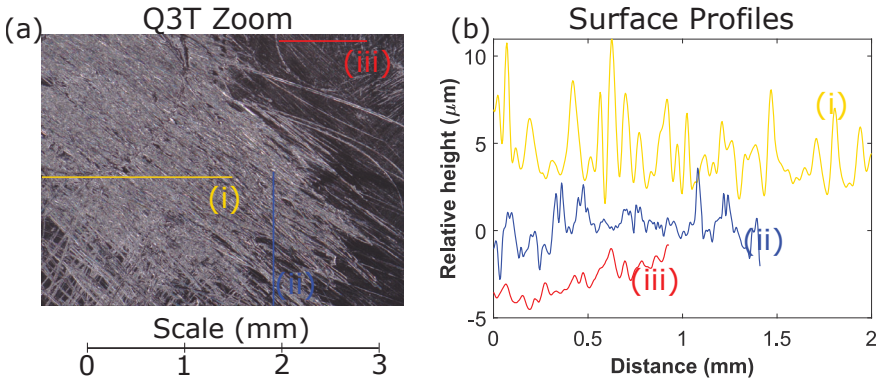

Figure 30: Surface roughness in quadrant 3 near the leading edge trip. (a) The same photograph from Fig. 9 with profiles defined across the roughness. (b) The height across the profiles defined in (a).

REPORT DOCUMENTATION PAGE

Form Approved
OMB No. 0704–0188

1. REPORT DATE *(DD-MM-YYYY)*	2. REPORT TYPE	3. DATES COVERED *(From - To)*
01-01-2023	Technical Memorandum	

4. TITLE AND SUBTITLE
BOLT II Forebody Surface Measurement Analysis

5a. CONTRACT NUMBER

5b. GRANT NUMBER

5c. PROGRAM ELEMENT NUMBER

6. AUTHOR(S)
Leidy, A. N.

5d. PROJECT NUMBER

5e. TASK NUMBER

5f. WORK UNIT NUMBER

7. PERFORMING ORGANIZATION NAME(S) AND ADDRESS(ES)
NASA Langley Research Center
Hampton, Virginia 23681-2199

8. PERFORMING ORGANIZATION REPORT NUMBER

9. SPONSORING/MONITORING AGENCY NAME(S) AND ADDRESS(ES)
National Aeronautics and Space Administration
Washington, DC 20546-0001

10. SPONSOR/MONITOR'S ACRONYM(S)
NASA

11. SPONSOR/MONITOR'S REPORT NUMBER(S)
NASA/TM–20230000169

12. DISTRIBUTION/AVAILABILITY STATEMENT
Unclassified-Unlimited
Subject Category 64
Availability: NASA STI Program (757) 864-9658

13. SUPPLEMENTARY NOTES
An electronic version can be found at http://ntrs.nasa.gov.

14. ABSTRACT

Surface impression molds of the nosetip/forebody interface, discrete tripping elements, and other surface imperfections were formed on the BOLT II flight vehicle prior to its launch in March 2022. The silicon-rubber molds cast on the interface between the nickel nosetip and the stainless steel forebody were measured using a 3D optical measurement system and a stylus profilometer and were evaluated for step direction and height. The step around the nosetip/forebody interface was found to vary in both magnitude and direction, but values were generally modest with most samples below 60 μm across the span and only two samples, both cast in the gutter, with step values larger than 100 μm. Impressions of the secondary-side tripping elements were strictly scanned with the optical device and similar methods were used to calculate trip height as step height. The measured centerline trip height was 2623 ±12 μm, while the leading-edge, quadrant 2 and 3, trip heights were 897 ±5 μm and 891 ±18 μm, respectively. Surface imperfections on the nose and forebody were also evaluated. Surface roughness values and spectra were estimated, and profiles were extracted across the imperfections to quantify the magnitude of those features.

15. SUBJECT TERMS
profilometry, step height, trip height, BOLT II, boundary layer transition, turbulence

16. SECURITY CLASSIFICATION OF:			17. LIMITATION OF ABSTRACT	18. NUMBER OF PAGES	19a. NAME OF RESPONSIBLE PERSON
a. REPORT	b. ABSTRACT	c. THIS PAGE			STI Information Desk (help@sti.nasa.gov)
U	U	U	UU	34	19b. TELEPHONE NUMBER *(Include area code)* (757) 864-9658

Standard Form 298 (Rev. 8/98)
Prescribed by ANSI Std. Z39.18